J. Fluid Mech. (2024), *vol*. 989, A15, doi:10.1017/jfm.2024.519

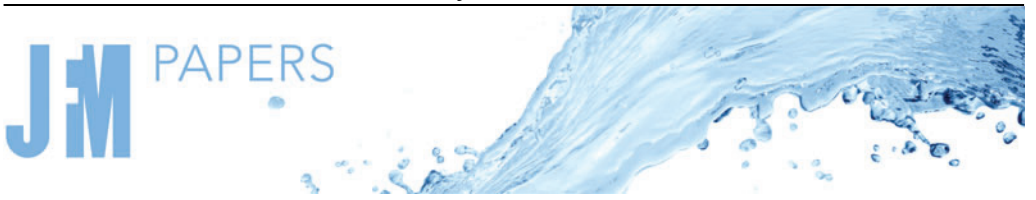

Wall-wake laws for the mean velocity and the turbulence

Alexander J. Smits†

Department of Mechanical and Aerospace Engineering, Princeton University, Princeton, NJ 08544, USA

(Received 2 February 2024; revised 7 April 2024; accepted 20 May 2024)

A new wall-wake law is proposed for the streamwise turbulence in the outer region of a turbulent boundary layer. The formulation pairs the logarithmic part of the profile (with a slope A_1 and additive constant B_1) to an outer linear part, and it accurately describes over 95 % of the boundary layer profile at high Reynolds numbers. Once the slope A_1 is fixed, B_1 is the only free parameter determining the fit. Most importantly, B_1 is shown to follow the same trend with Reynolds number as the wake factor in the wall-wake law for the mean velocity, which is tied to changes in scaling of the mean flow and the turbulence that occur at low Reynolds number.

Key words: turbulent boundary layers, boundary layer structure

1. Introduction

The mean velocity distribution in the outer part of a turbulent boundary layer is often expressed as a combination of a logarithmic part and a wake component, as in

$$\frac{U}{u_\tau} = \frac{1}{\kappa}\ln\frac{yu_\tau}{\nu} + B + \frac{2\Pi}{\kappa}W\left(\frac{y}{\delta}\right), \tag{1.1}$$

where U is the mean velocity in the streamwise direction, $u_\tau = \sqrt{\tau_w/\rho}$, τ_w is the shear stress at the wall where $y = 0$, ρ is the fluid density, κ is von Kármán's constant, B is the additive constant and Π is the Reynolds-number-dependent wake factor. The wake function W is taken to be a universal function of y/δ, where δ is the outer layer length scale. This wall-wake model was first formulated by Coles (1956), and it is an essential part of the widely used composite profile derived by Chauhan, Nagib & Monkewitz (2007).

† Email address for correspondence: asmits@princeton.edu

Marusic, Uddin & Perry (1997) proposed a similar formulation for the streamwise turbulence intensity in zero pressure gradient turbulent boundary layers, given by

$$\overline{u^2}^+ = B_1 - A_1 \ln \frac{y}{\delta_m} - V_g\left(y^+, \frac{y}{\delta_m}\right) - W_g\left(\frac{y}{\delta_m}\right), \tag{1.2}$$

where $\overline{u^2}^+ = \overline{u^2}/u_\tau^2$. The model incorporates the log-law for $\overline{u^2}^+$ with constants A_1 and B_1 (Hultmark *et al.* 2012; Marusic *et al.* 2013), where V_g is a mixed scale viscous deviation term, W_g is the wake deviation term and δ_m is a boundary layer thickness defined in a way that is similar to the Rotta–Clauser thickness. It is typically 15 % to 20 % larger than δ_{99}, the 99 % thickness (further details are given in Appendix A). The wake deviation was given by

$$W_g = B_1\eta^2(3 - 2\eta) - A_1\eta^2(1 - \eta)(1 - 2\eta), \tag{1.3}$$

where $\eta = y/\delta_m$. A more recent and simpler version of V_g was given by Baars & Marusic (2020) as

$$V_g = K_1 - K_2/\sqrt{y^+}, \tag{1.4}$$

with $K_1 = 4.01$, $K_2 = 10.13$.

Pirozzoli & Smits (2023) proposed an alternative model for the mean velocity distribution in the outer layer, given by a compound logarithmic–parabolic distribution of the type first suggested by Hama (1954); that is,

$$\frac{U_e - U}{u_\tau} = B' - \frac{1}{k_0}\ln\frac{y}{\delta_0}, \tag{1.5}$$

$$\frac{U_e - U}{u_\tau} = C\left(1 - \frac{y}{\delta_0}\right)^2, \tag{1.6}$$

where C is a constant, and U_e is the free stream velocity. Requiring the two velocity distributions to smoothly connect up to the first derivative yields the position of the matching point ($\eta_0 = y_0/\delta_0$) and the additive constant B' in (1.5) as a function of k_0 and C,

$$\eta_0 = \frac{1}{2}\left(1 - \left(1 - \frac{2}{Ck_0}\right)^{1/2}\right), \quad B' = C(1 - \eta_0)^2 + \frac{1}{k_0}\ln\eta_0. \tag{1.7a,b}$$

The matching point η_0 marks the outer limit of the logarithmic part, (1.5), and the inner limit of the wake part, (1.6). By comparing (1.1) with this compound model, and adopting Coles's wake function which has a maximum at $y/\delta_{99} = 1$, we find that $B' = 2\Pi/\kappa$, so that B' and Π are synonymous with each other. In what they called the classical case, Pirozzoli & Smits (2023) found that with $\delta_0 = 1.6\delta_{95}$ the best fit of the data was obtained with $k_0 = \kappa \approx 0.38$, $C \approx 9.88$, so that $B' = 2.15$, with the two distributions smoothly matched at $\eta_0 = 0.158$. This compound logarithmic–parabolic distribution fits the velocity distributions well down to $y/\delta_0 \approx 0.01$ (for Reynolds numbers based on displacement thickness greater than 2000).

Here, we suggest a similar approach for the streamwise component of the turbulent stress. That is, we propose a compound representation given by

$$\overline{u^2}^+ = B_1 - A_1 \ln \frac{y}{\delta_1}, \tag{1.8}$$

$$\overline{u^2}^+ = b_1 - a_1 \frac{y}{\delta_1}, \tag{1.9}$$

where a_1 and b_1 are constants, and δ_1 is the appropriate length scale for the outer layer. In this formulation, there is no viscous deviation term. Requiring the two turbulence distributions to smoothly connect up to the first derivative yields the position of the matching point ($\eta_1 = y_1/\delta_1$) and the additive constant B_1 in (1.8) as a function of the other constants,

$$\eta_1 = \frac{A_1}{a_1}, \quad B_1 = b_1 - A_1(1 - \ln \eta_1). \tag{1.10a,b}$$

The matching point η_1 marks the outer limit of the logarithmic part, (1.8), and the inner limit of the wake part, (1.9). According to (1.9), $\overline{u^2}^+$ is zero when $y/\delta_1 = b_1/a_1$, and so we impose one further constraint and set $b_1/a_1 = 1.05$ (which closely corresponds to the point where $y/\delta_{995} = 1$). Finally, if we assume A_1 is a true constant (= 1.26 for boundary layers according to Marusic *et al.* (2013)), the only free parameter in our fit to the turbulence profile is B_1, which we will show to be a Reynolds-number-dependent turbulence wake factor that behaves similarly to that of the mean velocity wake factor $B' = 2\Pi/\kappa$.

2. Comparisons with data

We now demonstrate the quality of the model by comparing it with experimental and direct numerical simulation data over a wide range of Reynolds numbers (see table 1). Before proceeding, we need to specify the particular length scale δ_1 used to describe the outer layer. We have chosen $\delta_1 = \delta_{99}$, for reasons made clear in Appendix A. We also need to relate $Re_\theta = \theta U_e/\nu$, where θ is the momentum thickness, to the friction Reynolds number $Re_\tau = \delta_{99} u_\tau/\nu$, in that not all data sets specify both. This issue is also addressed in Appendix A.

To begin the analysis, we use the data by Samie *et al.* (2018) ($6250 < Re_\theta < 47\,100$). Figure 1 demonstrates that, as expected from previous work, the logarithmic part with $A_1 = 1.26$ and $B_1 = 2.00$ is a good fit in the overlap region. In addition, the linear part of the model describes the profile beyond the matching point very well over this range of Reynolds numbers, except for the region $y/\delta_{99} > 1$ where a more gradual decline is observed. At the highest Reynolds numbers, the compound formulation represents the data well for 95 % of the profile.

For reference, we also plot (1.2) for the same values of A_1 and B_1 (using $\delta_{99}/\delta_m = 0.81$). We neglected the viscous deviation term V_g, which leads to a small positive offset of $\overline{u^2}^+$ in (1.2) with respect to the compound formulation in the logarithmic region. Both fits work well beyond the logarithmic region, although it could be argued that the linear fit is a trifle more accurate for $0.2 < y/\delta_{99} < 0.9$. In the analysis going forward, we will use the compound fit, primarily because the viscous deviation term in (1.2) appears to obscure some of the underlying trends as well as the comparisons between the turbulence and mean velocity profiles.

We now consider all the high-Reynolds-number data listed in table 1 over the range $6000 \leq Re_\theta < 60\,000$. The results are shown in figure 2 for $B_1 = 2.00$. Although there is

	Re_θ	Re_τ	b_1	B_1	η_1	η_1^+	Symbol
DeGraaff & Eaton (2000)	1430	541	3.56	1.05	0.372	201	●
	2900	993	3.77	1.19	0.351	349	■
	5200	1692	4.33	1.57	0.306	518	▲
	13 000	4336	4.83	1.94	0.274	1188	♦
	31 000	10 023	4.67	1.82	0.276	2766	○
Fernholz *et al.* (1995)	2573	866	4.10	1.42	0.323	280	•
	5023	1692	4.34	1.59	0.305	516	■
	7140	2375	4.80	1.92	0.276	656	▲
	16 080	5068	5.30	2.29	0.250	1267	♦
	20 920	6824	4.75	1.88	0.279	1904	○
	41 300	12 633	4.75	1.88	0.279	3524	□
	57 720	18 692	4.95	2.03	0.267	4991	△
	60 810	18 362	4.95	2.03	0.267	4903	◇
Osaka, Kameda & Mochizuki (1998)	6040	1800	4.75	1.88	0.279	502	●
Vallikivi, Hultmark & Smits (2015)	8402	2622	4.90	1.99	0.270	708	●
	15 121	4635	5.00	2.07	0.265	1228	■
	26 884	8261	4.85	1.95	0.273	2255	▲
	46 732	14 717	4.80	1.92	0.276	4061	♦
Samie *et al.* (2018)	6252	1929	4.92	2.00	0.269	519	●
	12 913	3984	4.96	2.04	0.267	1064	■
	26 034	8032	5.10	2.14	0.259	2080	▲
	47 096	14 530	4.88	1.98	0.271	3938	♦
Sillero, Jiménez & Moser (2013)	6000	1848	4.530	1.72	0.292	540	- - - -

Table 1. Data sources and fitting parameters for $A_1 = 1.26$. Here B_1 is the only free parameter, and b_1 and the matching point η_1 are defined by (1.10*a*,*b*).

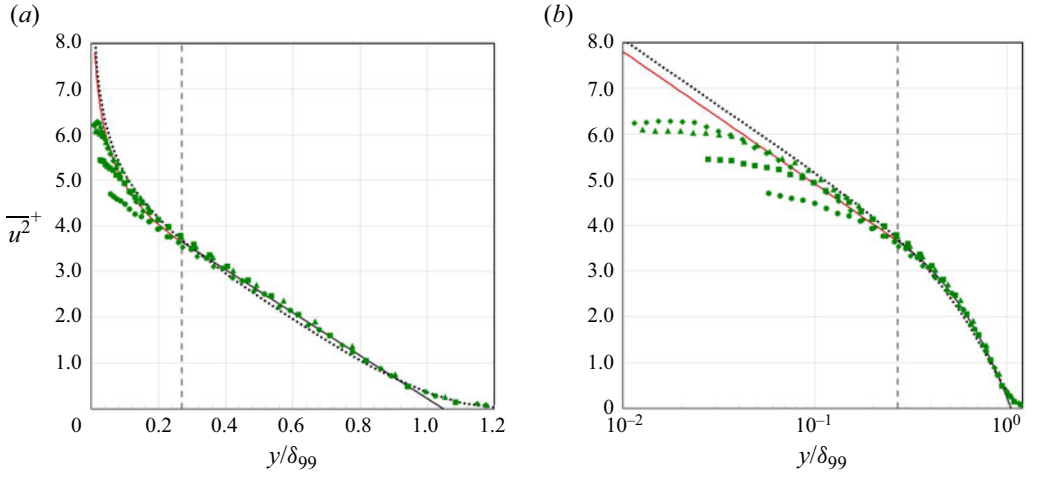

Figure 1. Comparison with the experimental data of Samie *et al.* (2018) for $Re_\theta = 6252$–$47\,096$ ($y^+ > 100$, $A_1 = 1.26$, $B_1 = 2.00$): (*a*) linear scaling; (*b*) logarithmic scaling. Here ·····, black, (1.2) (neglecting V_g); ———, red, (1.8); ———, black, (1.9) (matched at $\eta_1 = 0.269$, vertical dashed line). Symbols as in table 1.

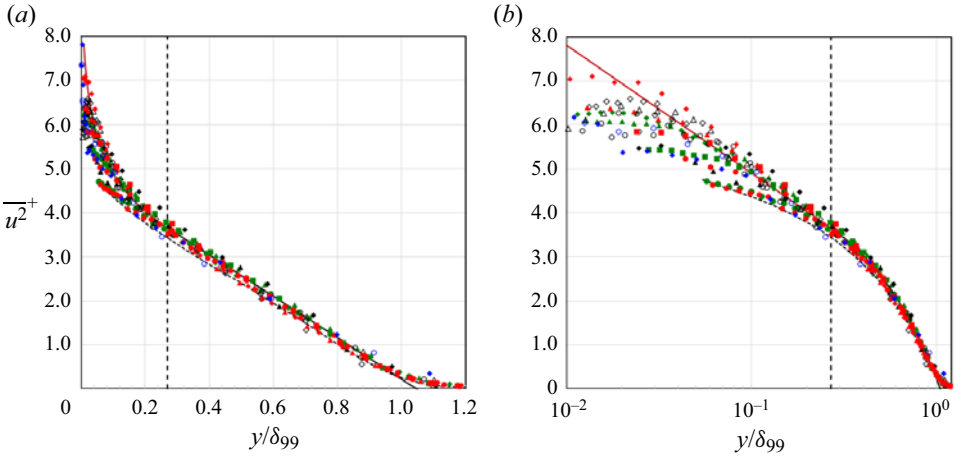

Figure 2. Comparison with all the experimental data for $6000 \leq Re_\theta < 60\,000$ ($y^+ > 100$): (*a*) linear scaling; (*b*) logarithmic scaling. Here ———, black, (1.9); ———, red, (1.8). $B_1 = 2.00$, distributions matched at $\eta_1 = 0.269$ (vertical dashed line). Symbols as in table 1.

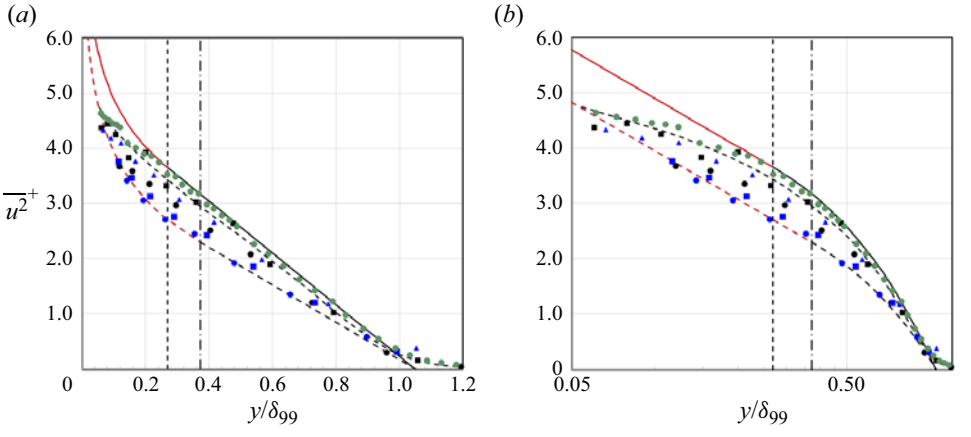

Figure 3. Comparison with the experimental data for $Re_\theta \leq 6040$ ($y^+ > 100$): (*a*) linear scaling; (*b*) logarithmic scaling. Here ———, black, (1.9); ———, red, (1.8). Here $b_1 = 4.92$, distributions matched at $\eta_1 = 0.269$ (vertical dashed line). Here - - - -, black, (1.9); - - - -, red, (1.8). Here $b_1 = 3.56$, distributions matched at $\eta_1 = 0.372$ (vertical dashed-dotted line). Symbols as in table 1

some the scatter in the data, the compound fit works reasonably well using this value. The agreement can be improved by using values of B_1 optimized for each profile, as listed in table 1.

The low-Reynolds-number data ($Re_\theta \leq 6040$) are shown in figure 3. The compound fit is plotted for two cases, $B_1 = 2.00$ (the value used for the high-Reynolds-number data shown in figures 1 and 2), and $B_1 = 1.05$ (chosen to match the lowest-Reynolds-number profile in the data set). In order to match the in-between Reynolds number cases, B_1 was varied as given in table 1. Again, we see a very satisfactory fit to the data, even in this low-Reynolds-number range.

The constant B_1 appears to act as a wake function for the turbulence profile, similar to the wake function Π for the mean velocity profile. In figure 4, we compare the Reynolds

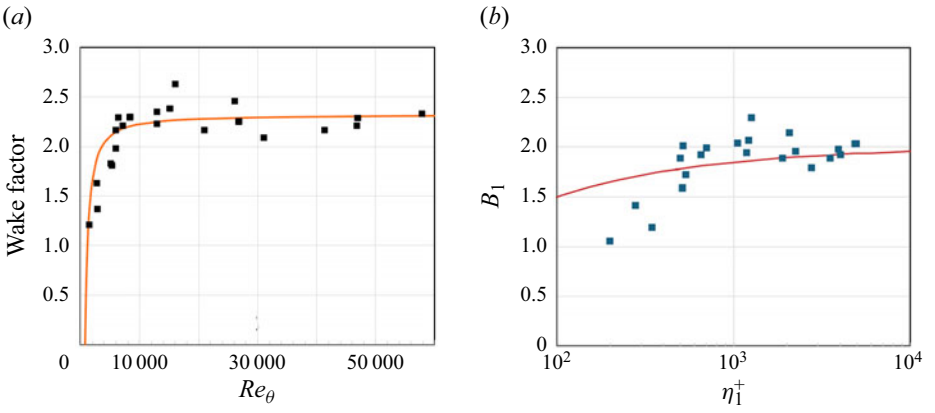

Figure 4. (*a*) Wake factors versus Re_θ. Here ■, black, $1.15B_1$; ———, red, $B' = 2\Pi/\kappa$ (Chauhan *et al.* 2007). (*b*) Turbulence wake factor B_1 as a function of η_1^+. Red line is $2V_g$ evaluated at η_1^+ (1.4).

number dependence of B_1 with that of $2\Pi/\kappa$ (using $\kappa = 0.384$, where B_1 was scaled by an arbitrary factor of 1.15 to aid the comparison. We see a clear similarity in the behaviour of the two wake functions, in that they increase with Reynolds number up to $Re_\theta \approx 6000$, and then become constant at higher Reynolds numbers.

To investigate this connection further, we first consider the wake factor $B' = 2\Pi/\kappa$ for the mean velocity. Now, B' is usually measured as the maximum deviation of the mean velocity profile from the log-law. For high-Reynolds-number flows ($Re_\theta > 6000$, $Re_\tau > 1800$), this gives a constant value, as seen in figure 4. However, at low Reynolds numbers ($Re_\tau \lessapprox 1300$), the log-law ceases to exist and it is replaced by a power law (Zagarola & Smits 1998*a*,*b*), and B' begins to decrease. It is suggested here that the decrease in B' at low Reynolds numbers is a result of incorrectly using a log-law to measure it at Reynolds numbers where no log-law exists.

As for the turbulence, the wake factor B_1 is the offset of the turbulence profile from its logarithmic variation. At high Reynolds numbers, B_1 is a constant, as seen in figure 4, but for $Re_\tau \lessapprox 2000$ the turbulence log-law (with constant A_1 and B_1) is usually assumed to vanish (Hultmark *et al.* 2012; Marusic *et al.* 2013). However, when we allow B_1 to vary with Reynolds number, we see that a logarithmic variation in the turbulence appears to be maintained, even at low Reynolds numbers.

This Reynolds number dependence of B_1 suggests that there may be a link to the viscous deviation term V_g, (1.4), in that they both embody the effects of viscosity. One way to explore this connection is to see how B_1 varies with $\eta_1^+ = \eta_1 u_\tau/\nu$ (see table 1). From figure 1, we see that B_1 begins to decrease quite sharply for $\eta_1^+ < 500$. We also show the value of V_g (as given by Baars & Marusic (2020)) at the matching point, and the trend in B1 is noticeably more severe than that of V_g.

We suggest, therefore, that the similarity between the Reynolds number dependence of B' and B_1 is a direct result of changes in the scaling behaviour of the mean velocity and turbulence profiles at low Reynolds number. In the first case, the log-law is replaced by a power law, and in the second case the slope of the logarithmic behaviour A_1 appears to remain constant while its intercept B_1 decreases. In that A_1 remains constant, it would indicate that the turbulence continues to obey the attached eddy scaling of y^{-1}, even at low Reynolds numbers (see Smits (2022) for further details).

3. Conclusions and discussion

The logarithmic–linear compound fit in y/δ_{99} proposed here for the streamwise turbulent stress $\overline{u^2}^+$ in the outer layer of a turbulent boundary layer works well over a wide range of Reynolds numbers. For the logarithmic part of the fit we assumed that A_1, the slope of the log-law, is fixed at 1.26 (as given by Marusic *et al.* (2013)), and the linear part of the fit was constrained to pass through zero at $y/\delta_{99} = 1.05$. As a consequence, the fit has only one free parameter, B_1, which acts like a wake factor.

For low Reynolds numbers ($Re_\theta \leq 6040$), B_1 increases with increasing Reynolds number, attaining an approximately constant value of approximately 2 for high Reynolds numbers ($6000 \leq Re_\theta \leq 60\,000$). At low Reynolds numbers ($Re_\theta < 6000$), B_1 decreases with decreasing Reynolds number. The behaviour of B_1 with Reynolds number closely follows the variation of the mean flow wake factor $B' = 2\Pi/\kappa$, and we propose that this is a direct result of changes in the scaling behaviour of the mean velocity and turbulence profiles at low Reynolds number: for the mean velocity the log-law is replaced by a power law, and for the turbulence the log-law intercept is Reynolds number dependent while it continues to obey the attached eddy wall-normal dependence.

For the logarithmic parts of the mean velocity and the turbulence distributions, we know that we can connect the behaviour of B' and B_1 through the attached eddy hypothesis (Perry & Chong 1982; Marusic & Monty 2019). For the parabolic part of the mean velocity, (1.6), and the linear part of the turbulence, (1.9), the link is still unknown. One possibility is to consider the behaviour of the 'detached' (or Type B) eddies (Perry & Marusic 1995). However, as they note, building this connection 'would be very complicated and would depend on the assumed shape of the representative eddies'. Also, as Hu, Yang & Zheng (2020) point out, 'unlike the attached eddies, whose statistical behaviours are well described by the (attached eddy hypothesis), the detached eddies lack a good phenomenological model'. Building a better understanding of the physics that connects the mean velocity and the turbulence in the outer layer is clearly in need of further work.

Acknowledgements. The authors would like to thank S. Pirozzoli and J.-P. Dussauge for their comments on an earlier draft.

Declaration of interests. The author reports no conflict of interest.

Author ORCIDs.
Alexander J. Smits https://orcid.org/0000-0002-3883-8648.

Appendix A. Data analysis

For the length scale used to describe the outer layer, δ_1, there are a multitude of choices. In examining the mean flow, Pirozzoli & Smits (2023) considered $\delta_0 = 1.6\delta_{95}$, 0.28Δ and $2\delta_N$, where $\Delta = (U_e/u_\tau)\delta^*$ is the Rotta–Clauser thickness, δ^* is the displacement thickness, $\delta_N = (H/(H-1))\delta^*$ and $H = \delta^*/\theta$ is the shape parameter. For the data in table 1, Sillero *et al.* (2013), DeGraaff & Eaton (2000) and Vallikivi *et al.* (2015) used δ_{99}, Osaka *et al.* (1998) used δ_{995}, and Samie *et al.* (2018) used δ_c, where δ_c is the outer length scale adopted by Chauhan *et al.* (2007) for their composite profile. In order to compare data, we need a common standard, and we will show that $\delta_1 = \delta_{99}$ serves that purpose well. To convert δ_{995} and δ_c to the matching value of δ_{99}, we used the composite profile. In figure 5, we show how these various thicknesses compare.

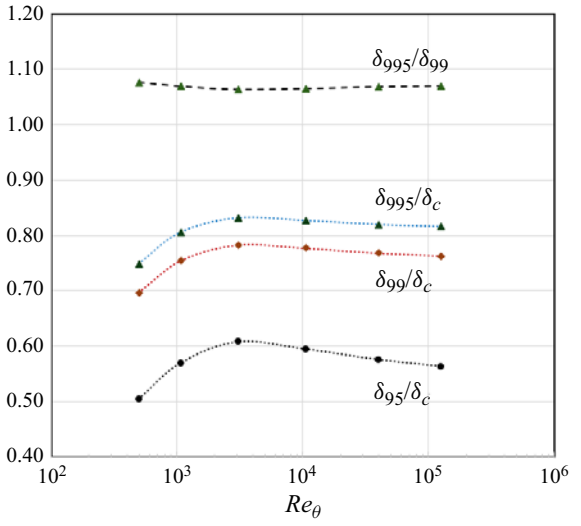

Figure 5. Boundary layer thickness variations with Re_θ, as found using the composite profile (Chauhan *et al.* 2007).

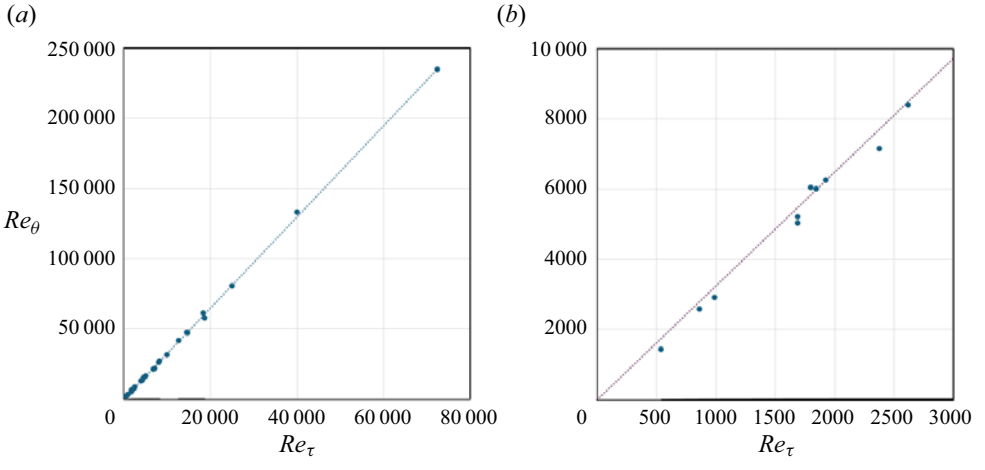

Figure 6. Momentum thickness Reynolds number versus friction Reynolds number: dashed line, (A1); (*a*) full data set; (*b*) data for $Re_\theta < 10\,000$.

We used the results of Klebanoff (1955) on the eddy viscosity. His boundary layer thickness was approximately 1.15 times larger than δ_{99} (Smits 2024), and the data were scaled accordingly.

In addition, we need to relate Re_θ and Re_τ, in that not all data sets specify both. Here, we use

$$Re_\theta = 3.241 Re_\tau, \tag{A1}$$

based on a fit to the available data ($R^2 = 0.9997$ for full data set), see figure 6.

Finally, the $Re_\theta = 234\,670$ profile by Vallikivi *et al.* (2015) was corrected for an error in the 99 % thickness, which was smaller by a factor of 0.943 than the value originally reported. This changed the profile, and the corresponding value of Re_τ. Also, the Fernholz profile at $Re_\theta = 21\,410$ was not used since it has some obvious problems.

References

Baars, W.J. & Marusic, I. 2020 Data-driven decomposition of the streamwise turbulence kinetic energy in boundary layers. Part 2. Integrated energy and A_1. *J. Fluid Mech.* **882**, A26.

Chauhan, K., Nagib, H. & Monkewitz, P. 2007 On the composite logarithmic profile in zero pressure gradient turbulent boundary layers. *AIAA Paper* 2007-0532.

Coles, D.E. 1956 The law of the wake in the turbulent boundary layer. *J. Fluid Mech.* **1**, 191–226.

DeGraaff, D.B. & Eaton, J.K. 2000 Reynolds-number scaling of the flat-plate turbulent boundary layer. *J. Fluid Mech.* **422**, 319–346.

Fernholz, H.H., Krause, E., Nockemann, N. & Schober, M. 1995 Comparative measurements in the canonical boundary layer at $Re_{\delta_2} \leq 6 \times 10^4$ on the wall of the German-Dutch windtunnel. *Phys. Fluids* **7**, 1275–1281.

Hama, F.R. 1954 Boundary layer characteristics for smooth and rough surfaces. *Trans. Soc. Nav. Archit. Mar. Engrs* **62**, 333–358.

Hu, R., Yang, X.I.A. & Zheng, X. 2020 Wall-attached and wall-detached eddies in wall-bounded turbulent flows. *J. Fluid Mech.* **885**, A30.

Hultmark, M., Vallikivi, M., Bailey, S.C.C. & Smits, A.J. 2012 Turbulent pipe flow at extreme Reynolds numbers. *Phys. Rev. Lett.* **108** (9), 1–5.

Klebanoff, P.S. 1955 Characteristics of turbulence in a boundary layer with zero pressure gradient. NACA Report 1247. National Advisory Committee for Aeronautics.

Marusic, I. & Monty, J.P. 2019 Attached eddy model of wall turbulence. *Annu. Rev. Fluid Mech.* **51**, 49–74.

Marusic, I., Monty, J.P., Hultmark, M. & Smits, A.J. 2013 On the logarithmic region in wall turbulence. *J. Fluid Mech.* **716**, R3.

Marusic, I., Uddin, M. & Perry, A.E. 1997 Similarity law for the streamwise turbulence intensity in zero-pressure-gradient turbulent boundary layers. *Phys. Fluids* **12**, 3718–3726.

Osaka, H., Kameda, T. & Mochizuki, S. 1998 Re-examination of the Reynolds-number-effect on the mean flow quantities in a smooth wall turbulent boundary layer. *JSME Intl J.* B **41** (1), 123–129.

Perry, A.E. & Chong, M.S. 1982 On the mechanism of wall turbulence. *J. Fluid Mech.* **119**, 173–217.

Perry, A.E. & Marusic, I. 1995 A wall-wake model for the turbulence structure of boundary layers. Part 1. Extension of the attached eddy hypothesis. *J. Fluid Mech.* **298**, 361–388.

Pirozzoli, S. & Smits, A.J. 2023 Outer-layer universality of the mean velocity profile in turbulent wall-bounded flows. *Phys. Rev. Fluids* **8** (6), 064607.

Samie, M., Marusic, I., Hutchins, N., Fu, M.K., Fan, Y., Hultmark, M. & Smits, A.J. 2018 Fully resolved measurements of turbulent boundary layer flows up to $Re_\tau = 20\,000$. *J. Fluid Mech.* **851**, 391–415.

Sillero, J.A., Jiménez, J. & Moser, R.D. 2013 One-point statistics for turbulent wall-bounded flows at Reynolds numbers up to $\delta^+ \approx 2000$. *Phys. Fluids* **25** (10), 105102.

Smits, A.J. 2022 Batchelor prize lecture: measurements in wall-bounded turbulence. *J. Fluid Mech.* **940**, A1.

Smits, A.J. 2024 Assessing Klebanoff's data. *Exp. Fluids* **65**, 62.

Vallikivi, M., Hultmark, M. & Smits, A.J. 2015 Turbulent boundary layer statistics at very high Reynolds number. *J. Fluid Mech.* **779**, 371–389.

Zagarola, M.V. & Smits, A.J. 1998*a* Mean-flow scaling of turbulent pipe flow. *J. Fluid Mech.* **373**, 33–79.

Zagarola, M.V. & Smits, A.J. 1998*b* A new mean velocity scaling for turbulent boundary layers. *ASME paper FEDSM98-4950*.